Inorganic Chemistry
Article
Cite This: Inorg. Chem. 2019, 58, 2848−2855
pubs.acs.org/IC

Pseudogap Control of Physical and Chemical Properties in CeFeSi-Type Intermetallics

Jiazhen Wu,[†,⊥] Erdong Lu,[‡,⊥] Jiang Li,[†] Yangfan Lu,[†] Masaaki Kitano,[†] Daniel C. Fredrickson,*[,†,‡] Takeshi Inoshita,[†,§] and Hideo Hosono*[,†,∥]

[†]Materials Research Center for Element Strategy, Tokyo Institute of Technology, 4259 Nagatsuta, Midori-ku, Yokohama 226-8503, Japan

[‡]Department of Chemistry, University of Wisconsin—Madison, 1101 University Avenue, Madison, Wisconsin 57306, United States

[§]National Institute for Materials Science, Tsukuba, Ibaraki 305-0044, Japan

[∥]Laboratory for Materials and Structures, Institute of Innovative Research, Tokyo Institute of Technology, 4259 Nagatsuta, Midori-ku, Yokohama 226-8503, Japan

Supporting Information

ABSTRACT: We describe the synthesis of the new ternary compound CaRuSi whose chemical and physical properties help draw a clear picture of how electronic structure controls the behavior of an isostructural series of intermetallics. DFT calculations reveal that an electronic pseudogap arises near the Fermi level (E_F), corresponding to 14 valence electrons per RuSi unit. The closed-shell-like character is further investigated by comparisons with the electronic structures of CaCoSi (15 electrons), where the E_F lies above the corresponding pseudogap, and its hydride CaCoSiH, where formation of H anions restores the 14-electron count on the metal sublattice, returning the E_F to the pseudogap. The chemical origin of the 14-electron pseudogap is interpreted with a reversed approximation Molecular Orbital analysis. Here, the pseudogap is shown to coincide with the filling of Ru 16 electron configurations isolobal to the d^8 square planar complexes of coordination chemistry (but where 4 electron pairs are shared covalently between Ru atoms such that only 12 electrons are required), and the occupation of Si lone pairs (2 electrons). Experimentally, the pseudogap is confirmed with heat capacity measurements, which indicate that the 14-electron systems CaRuSi and CaCoSiH each exhibit a smaller electronic density of states at the E_F than the 15-electron system CaCoSi. Importantly, the 14-electron pseudogap also significantly affects the chemical properties of the compounds, as evidenced by the difference in the stabilities of CaCoSiH and CaRuSiH observed in hydrogen desorption measurements. These results may support the design of functional materials for superconductivity, hydrogen storage, and catalysis involving hydrogenation.

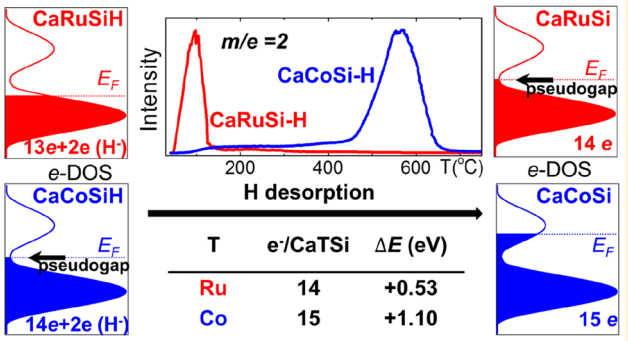

INTRODUCTION

Ternary compounds composed of an electropositive metal (A = alkali, alkaline earth, or rare earth metals), transition metals (T), and p-block elements (X) have illustrated how compounds with relatively simple and common structural motifs can give rise to a broad range of chemical and physical properties.[1−8] This diversity of behavior is perhaps most pronounced for the family of tetragonal structures with two-dimensional (2D) TX layers of TX_4 tetrahedra sandwiched by A_4-tetrahedral layers (space groups $I4/mmm$ and $P4/nmm$).[1,2] For example, in ATX compounds with rare earth metals on the A sites, the Kondo effect, heavy Fermion behavior, and intermediate valence have all been encountered, along with other phenomena.[1] The most well-known materials in this family and their derivatives are probably the "111", "1111", "122", and "11" phases of the iron-based superconductors, whose high critical temperatures (T_c's) point to a new mechanism for high-T_c superconductivity.[4−7]

ATX compounds also offer attractive chemical properties with the potential for useful applications. Hydrogen can be reversibly incorporated inside their A_4 tetrahedra, which modifies the crystal structures and local chemical environment as well as the associated magnetic and electronic properties.[1,8−11] Recently, we showed that the electride concept can be applied to these compounds and their use in catalysis.[12−14] Tiered electron anions have been associated with the La_4 tetrahedra and La_2Sc_4 octahedra in LaScSi, which work effectively to promote Ru for catalytic ammonia synthesis.[12] In fact, the replacement of Sc with late transition metals led to LaCoSi and $LaCu_{0.67}Si_{1.33}$, which act as self-promoted catalysts

Received: December 20, 2018
Published: February 7, 2019

DOI: 10.1021/acs.inorgchem.8b03539
Inorg. Chem. 2019, 58, 2848−2855

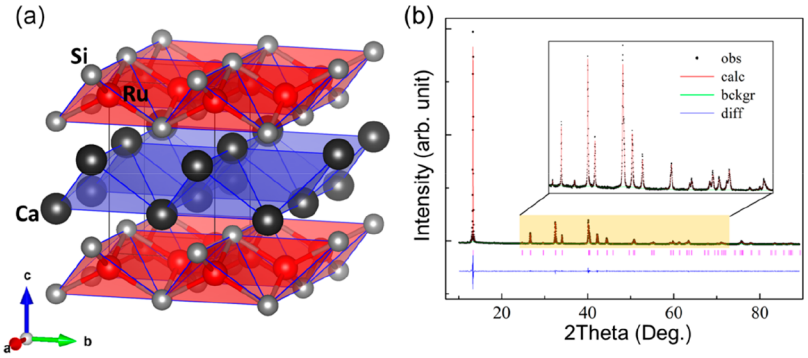

Figure 1. (a) Experimentally determined crystal structure of CaRuSi. (b) Powder X-ray diffraction pattern of CaRuSi and the simulated pattern from Rietveld refinement.[16−18]

for ammonia synthesis and chemoselective hydrogenation reactions, respectively.[13,14] Such results illustrate the rich potential of ATX compounds as functional materials, motivating the exploration of new phases and new functionalities in this family.

Herein, we report the synthesis of the new phase CaRuSi, which, in addition to being the first ternary phase in the Ca−Ru−Si system, provides a clear illustration of how electronic structure can control the properties of these materials. As with the other members in the ATX family, CaRuSi shows a quasi-2D character and a reversible hydrogen absorption/desorption behavior. By studying the electronic structures of CaRuSi, the recently reported CaCoSi phase,[15] and their hydride derivatives, we will see that the Fermi energies (E_F's) of the 14-electron systems CaRuSi and CaCoSiH lie near a pseudogap, while the E_F climbs above the corresponding pseudogap for the 15-electron system CaCoSi, in line with a rigid-band picture. The bonding optimization at 14-electrons per TX unit is further analyzed and interpreted by a reversed approximation Molecular Orbital (raMO) analysis, revealing connections to other transition-metal-containing intermetallics and square planar coordination complexes. Accordingly, the placement of the E_F relative to this pseudogap plays a dominant role in the differing properties of CaRuSi and CaCoSi, from their low-temperature heat capacities and electrical resistivities to their distinct affinities for hydrogen, as observed in the hydrogen desorption behavior of their hydrides.

EXPERIMENTAL SECTION

CaRuSi samples were synthesized using a solid state reaction route. First, a RuSi precursor was prepared by arc melting using a 1:1 ratio of Ru granules (99.9%, Rare Metallic Co., Ltd.) and Si pieces (99.99%, Kojundo Chemical Laboratory Co., Ltd.). Each sample was melted five times to achieve homogeneity. The RuSi ingot was next crushed and hand milled into a fine powder using an agate motor. The RuSi powder was then mixed with Ca pieces (99.9%, Sigma-Aldrich) and pressed into pellets, which were loaded into Ta crucibles that in turn were sealed inside Ar-filled quartz tubes. To compensate for the loss of Ca due to its vapor pressure, an excess amount of 5% was added. The mixture was heated in a box furnace at 850 °C for 10 h and then at 800 °C for 2 days, and finally cooled down to room temperature over 2 days. When low-density Ca reacts with RuSi, the total volume becomes smaller, so the obtained compound is fluffy and gray in color. CaRuSi powder was prepared by hand milling for X-ray diffraction experiments and further characterization. CaCoSi was synthesized using a similar method (Co: 99.9%, Kojundo Chemical Laboratory Co., Ltd.), but the obtained samples contained small amounts of impurity phases (Ca_2Si, CoSi, and CaO) as previously reported.[15]

Powder X-ray diffraction (XRD) measurements were performed using a Bruker D8 Advance X-ray powder diffractometer with Cu Kα radiation (λ = 1.5406 Å), and the results were analyzed with Rietveld refinement[16] using the GSAS package.[17,18] Electrical resistivity and heat capacity were measured with a physical properties measurement system (PPMS, Quantum Design). The sample for physical properties measurements was prepared by pelletizing the powder with a hydrostatic pressure of 200 MPa, and some pellets were annealed at 600 °C for 30 h.

Hydrogenation experiments were performed in a silica reactor at 75−400 °C under 1 bar of flowing hydrogen (extra pure, purity >99.99995%) for approximately 20 h. Hydrogen desorption measurements were conducted using thermal desorption spectroscopy (TDS, ESCO 1400TV) under high vacuum (pressure ~10^{-5}−10^{-7} Pa).

The band structures of CaRuSi, CaCoSi, CaRuSiH, and CaCoSiH were calculated with the Vienna ab initio Simulation Package (VASP)[19,20] using a plane-wave basis set and projector-augmented wave potentials[21,22] with a cutoff energy of 700 eV. The exchange-correlation potential was treated with the generalized gradient approximation (GGA) in the Perdew, Burke, and Ernzerhof (PBE) form.[23] The k-point mesh was set to 11 × 11 × 7, while for density of states (DOS) calculations, a finer mesh of 19 × 19 × 13 was used. The calculations were made on the basis of the experimentally obtained crystal structures.

For the reversed approximation Molecular Orbital (raMO) analyses, DFT-calibrated Hückel models were fit with the program eHtuner to the band energies and DOS distributions of geometrically[24] optimized structures of CaRuSi (6 × 6 × 3 Γ-centered mesh, energy cutoff: 306.8 eV) and CaCoSiH (finer 24 × 24 × 12 Γ-centered mesh to better see the pseudogap at E_F, energy cutoff: 335.0 eV). Hückel calculations were then performed with YAeHMOP on 5 × 5 × 2 supercells of the structures to map multiple k-points onto the Γ point. Finally, the Γ point Hamiltonian matrices were imported into MATLAB where the raMO analyses[25−27] were carried out with the in-house functions makeramo and raMOmovie. Further details regarding the calculations are provided in Tables S1−S5.

RESULTS AND DISCUSSION

Synthesis and Structure Determination of CaRuSi. As revealed by powder X-ray diffraction patterns, our syntheses resulted in essentially phase-pure samples of a CeFeSi-type CaRuSi phase with the tetragonal space group *P*4/*nmm*. The lattice parameters derived from the Rietveld refinement (a = 4.249 Å, c = 6.654 Å; see Table S6 for further details) are in agreement with those from a theoretical optimized structure (a = 4.269 Å, c = 6.673 Å). Analogous to other tetragonal ATX compounds, the CaRuSi structure is built from RuSi sheets of edge-sharing $RuSi_4$ tetrahedra separated by Ca double layers (Figure 1). During the Rietveld refinement, it was necessary to

DOI: 10.1021/acs.inorgchem.8b03539
Inorg. Chem. 2019, 58, 2848−2855

include a preference for grains to have plate-like sheets running perpendicular to the c axis. Scanning electron microscopy images support this model, showing that the samples exhibit a laminated morphology (Figure S1). This is easily interpretable in terms of the Ru−Si interactions being stronger than the Ca−Ca ones. Curiously, the c/a = 1.566 of CaRuSi is the smallest in the ATX family (Table S7). Two possible reasons are (1) the larger covalent radius of Ru compared to 3d transition metals (Mn, Fe, Co, Ni), giving rise to a larger lattice parameter a, and (2) the greater electronegativity of Ru (2.2) relative to those of Mn (1.55), Fe (1.83), Co (1.88), and Ni (1.91), leading to a stronger electrostatic attractive interaction between $[RuSi]^{2-}$ layers and Ca^{2+} layers along c and thus a smaller c parameter.

As emphasized in Figure 1a, the double layers of Ca atoms sandwiched between RuSi layers can be viewed as built from edge-sharing Ca_4 tetrahedra, a universal feature of tetragonal ATX compounds that can accommodate electrons or hydrogen atoms.[1,8−10,12,13] Indeed, after hydrogenation at 75 °C, we found that CaRuSi absorbs one hydrogen atom per formula unit (f.u.) to form CaRuSiH (Figure S2). While the lattice structure is not altered, the lattice was slightly compressed in the a and b directions but stretched by 13.5% in the c direction (Table S8), consistent with the hydrogen intercalating inside the Ca double layer. This lattice expansion under hydrogenation is the largest yet seen among the tetragonal ATX compounds.[2] Following the observations of other compounds in this family,[8,10,13] we suggest that the H atoms are inserted into the Ca_4 tetrahedra and occupy the 2b site (1/4, 3/4, 1/2) of the structure, though neutron diffraction experiments on deuteride samples would be necessary to make this assignment definitive. As hydrogen contains only one electron and thus has a small scattering factor, its influence on the X-ray diffraction data as well as the refinement is expected to be negligible. Therefore, in the Rietveld refinement, H was placed on the Wyckoff 2b site with its atomic displacement parameter (U_{eq}) set to the fixed value of 0.02. For comparison with the CaRuSi and its hydride in this study, CaCoSi and CaCoSiH were also synthesized in similar ways, with the powder X-ray diffraction analysis as well as the lattice parameters being given in the Supporting Information (Figures S3 and S4, and Tables S9 and S10).

Electronic Pseudogaps in CeFeSi-Type Phases. Clues to the electronic factors underlying these structural observations and the potential properties of CaRuSi are offered by its DFT electronic structure. In Figure 2a, we show the electronic density of states (DOS) calculated for this phase, where features familiar from other ATX compounds may be noted. The Fermi energy (E_F) lies just at the bottom of a pseudogap atop a series of peaks arising from bands based on the Ru 4d orbitals and their interactions with the Si (mainly Si 3p) that stretches to about −5 eV (relative to the E_F). Below this block, a separate collection of states appears from about −9.5 to −7.5 eV, corresponding to Si 3s-rich bands. The placement of the E_F near a DOS minimum is suggestive of the system having an optimized electron count at its 14 electrons per formula unit, while the absence of substantial contributions from the Ca in the occupied states affirms the view of CaTX compounds as built from $[TX]^{2-}$ sublattices stabilized by Ca^{2+} cations.[28]

For comparison, we plot the corresponding DOS curve calculated for CaCoSi in Figure 2b. As might be expected from its being isostructural to CaRuSi, DOS distributions of CaCoSi show largely analogous features. There are two key differences,

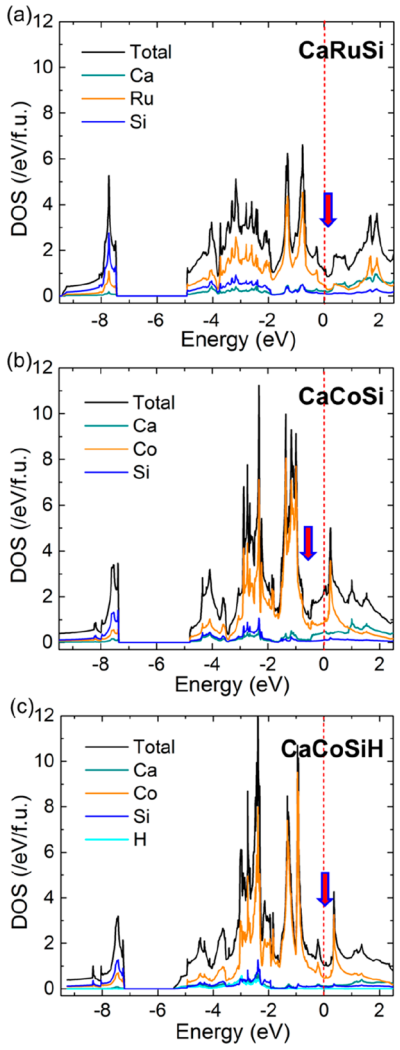

Figure 2. Electron density of states (DOS) distributions of (a) CaRuSi, (b) CaCoSi, and (c) CaCoSiH. The Fermi levels (E_F's) are shown by red dashed lines, and the pseudogap near the E_F in each case is indicated by an arrow.

however. First, the bandwidth for the Co-3d-based bands of CaCoSi is narrower than the Ru-4d-derived ones of CaRuSi (Figure 2), in line with the more contracted nature of the Co-3d orbitals. The second, and perhaps more important, difference is in the placement of the E_F's relative to the DOS minima. While for CaRuSi the E_F falls just at the bottom of the pseudogap (Figure 2a), in CaCoSi the E_F is shifted to 0.6 eV above the pseudogap in states with greater Ca contributions (Figure 2b). Interestingly, after hydrogenation to form CaCoSiH, the E_F shifts to align once again with the pseudogap (Figure 2c), similar to the situation of CaRuSi. This hints that hydrogenation can be considered to play the role of hole doping in CaCoSi, a theme we will soon return to. The band structures of CaRuSi, CaCoSi, and their hydrides are shown in Figure S5.

Analogous DOS minima can also be found in other isostructural 14-electron ATX systems, such as LiFeAs and MgFeGe,[29] suggesting that it is a universal feature of this structure. Along the same lines, electronic structure calculations on the 16-electron phase CaNiGe show that its E_F lies above the pseudogap,[28,30] as is the case for 15-electron systems, such as CaNiGeH[30] and CaCoSi in the present study.

DOI: 10.1021/acs.inorgchem.8b03539
Inorg. Chem. 2019, 58, 2848−2855

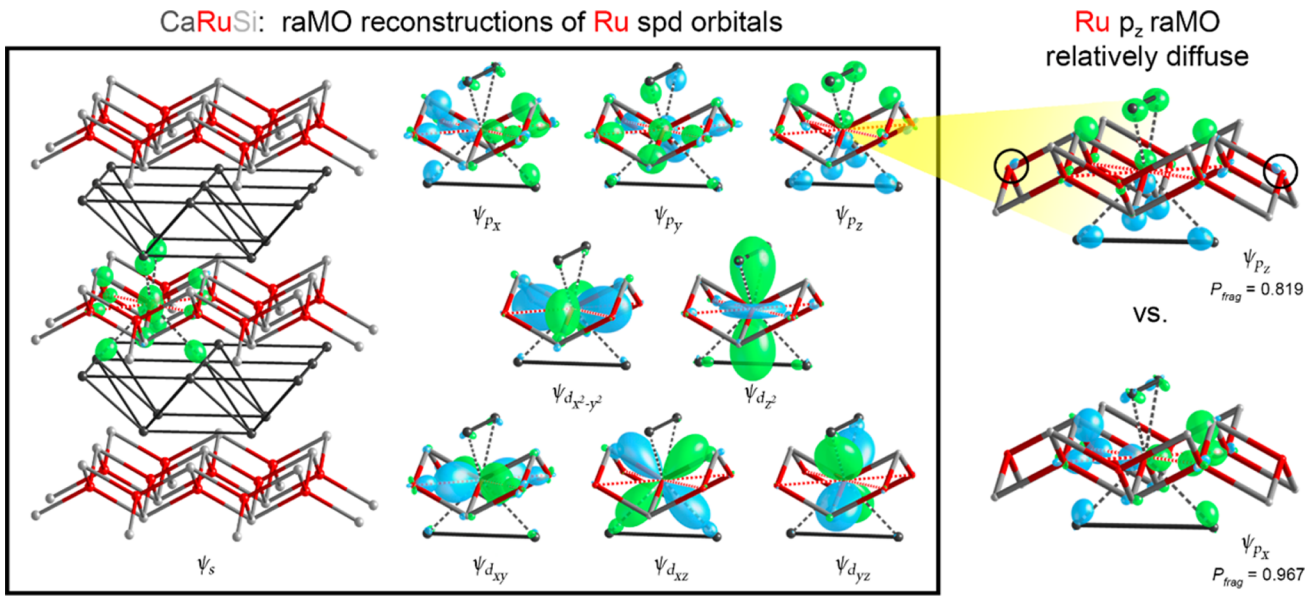

Figure 3. raMO reconstructions of a Ru atom's valence s, p, and d atomic orbitals in CaRuSi from a DFT-calibrated Hückel model. In the right panel, the relatively diffuse nature of the Ru p_z raMO is illustrated, with P_{frag} being defined as the probability that an electron occupying the raMO function lies within the fragment of the structure drawn.

Origins of the 14-Electron Pseudogap. The 14-electron pseudogap thus appears to be central to the electron structure of CeFeSi-type ATX compounds, but the question of why this particular electron count is associated with an opening in the DOS remains unanswered. A simple hypothesis is offered by the 18 − *n* rule for T-containing intermetallic phases: closed shell configurations are expected for a T atom when it is associated with 18 − *n* valence electrons, where *n* is the number of electron pairs that the T atom shares covalently with other T atoms in functions isolobal to classic T−T bonds.[26,31−33] Each T atom in the ATX structures described here has 4 T neighbors arranged in a square planar arrangement. If each of these T−T interactions is assigned an isolobal bond, closed shell electron configurations would be expected for 18 − 4 = 14 electrons per T atom, corresponding to the observed position of the pseudogap in the electronic structure of each compound. In order to test this notion, and trace the 14-electron pseudogap to particular structural features, we created DFT-calibrated Hückel models for the electronic structures of CaRuSi and CaCoSiH and analyzed them using the reversed approximation Molecular Orbital (raMO) method.[26]

For a T atom to have a filled 18-electron configuration, it should have an electron pair associated with each of its nine s, p, and d valence atomic orbitals. The raMO method offers a way of testing whether this applies to the T atoms of an ATX phase. Here, we use the fully occupied crystal orbitals of the compound as a basis set for the best possible reconstructions of the T atoms' s, p, and d orbitals that maintain orthogonality with each other. The result for one Ru atom in CaRuSi is shown in Figure 3. Here, the raMO functions for the Ru 4d orbitals appear tightly localized to the Ru centers, with some bonding contributions from the surrounding Ru, Si, and Ca atoms. Electron pairs are clearly associated with each of these orbitals. The Ru 5s, $5p_x$, and $5p_y$ orbitals are more delocalized throughout the Ru coordination environment, in accord with the higher energy of these atomic orbitals. However, each of the lobes from the neighboring atoms is clearly directed toward the Ru center; the Ru atom is the focal point for the electron pairs in these functions.

In contrast, the raMO for the Ru p_z orbital (oriented perpendicular to the RuSi sheet) shows substantial contributions for Si orbitals that point away from the Ru. In fact, a closer inspection of this function makes clear it is more delocalized through the structure than the other Ru 5p-based raMOs (right panel of Figure 3); the degree of localization of each orbital is shown in Figure S6. The electrons captured by this raMO may be better associated with another aspect of the structure.

Setting aside the Ru $5p_z$ orbital for now, we have found 16 electrons to be closely associated with the Ru center. The appearance of Ru−Ru bonding interactions in the raMO functions, however, indicates that this is achieved with the support of electron sharing between the Ru atoms. The Ru−Ru interactions are particularly strong in four of the raMOs: those based on the Ru 5s, $5p_x$, $5p_y$, and $4d_{xy}$. The presence of four bonding functions for four Ru−Ru contacts suggests the possibility for creating localized functions through linear combinations. In fact, the classic recipe for sp^2d hybridization can be followed to create functions localized to each Ru−Ru contact (and their bridging Si atoms), as illustrated in Figure 4. The existence of these four isolobal bonds is consistent with the 18 − *n* scheme. However, the absence of a clear electron pair on the $5p_z$ orbital means that the Ru atom is better described as having a 16 − *n* configuration. Apparently, the interactions with Ca neighbors directly above and below the Ru $5p_z$ orbital are not sufficiently strong to push this function below the E_F, leading to a situation that is closely analogous to square planar d^8 coordination complexes (which also follow a 16-electron scheme).[34] In this way, 16 − 4 = 12 of the 14 electrons per formula unit in the structure can be assigned to the Ru atoms.

Where are the remaining two electrons? The raMO reconstruction of the Ru $5p_z$ orbital provides clues here. It contains contributions from Si hybrid orbitals pointing outward from the Ru−Si layer, suggesting the existence of

DOI: 10.1021/acs.inorgchem.8b03539
Inorg. Chem. 2019, 58, 2848−2855

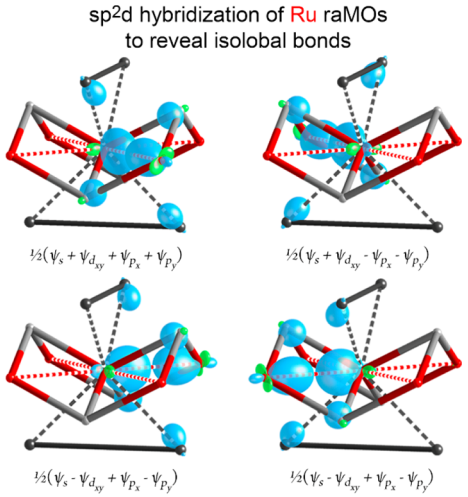

Figure 4. Linear combinations of the Ru-based raMOs involved in Ru−Ru bonding to create four Ru−Ru isolobal bonds.

lone pairs on the Si atom not associated with the Ru centers. To explore this possibility, we first reconstruct the full set of Ru-based functions assuming they follow the 16 − *n* scheme and then use the remaining states as a basis set for the construction of Si sp hybrid orbitals pointing directly away from the Ru−Si layer. The resulting raMO functions (Figure 5) closely resemble Si lone pairs with the correct orientation

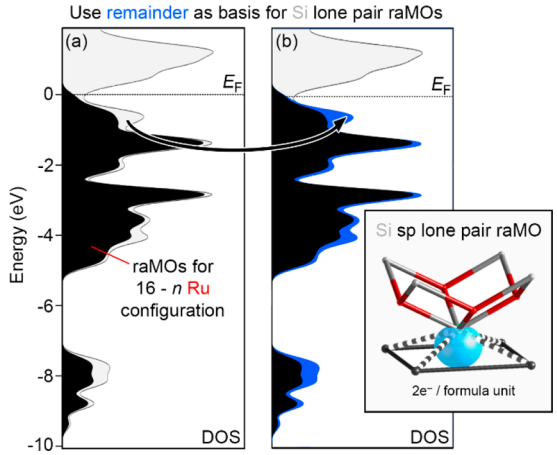

Figure 5. Completion of the bonding scheme of CaRuSi with the assignment of Si lone pairs. (a) DOS distribution with the contributions from the full set of Ru-centered raMOs shaded and the remainder states (corresponding to 2 electrons per formula unit) remaining unshaded. (b) raMO reconstruction of a Si sp lone pair from the remainder states in (a) and the contributions of such functions to the DOS (blue).

and are tightly localized to the Si. Placing such a lone pair on each Si atom requires 2 electrons per formula unit, which when added to the 12 electrons on the Ru leads us to the expected total count of 14 electrons per formula unit.

This overall bonding scheme also has correspondences in the electron localization function (ELF) analyses of CaNiGe and CaCoSi carried out previously, where maxima corresponding to Ge or Si lone pairs pointing out from the NiGe or CoSi layers were clearly visible, while for CaCoSi ELF peaks were also observed along the Co−Co contacts consistent with the importance of transition metal−transition metal interactions to the electron counting in these phases.[15,28]

Role of H Atoms in the Bonding of the Hydrogenated Derivatives. Our raMO analysis of CaRuSi indicates that the 14-electron pseudogap corresponds to the filling of Si lone pairs and Ru 16 − *n* configurations. We now turn to a raMO analysis of CaCoSiH to determine how this scheme changes upon the introduction of hydrogen. The reconstruction of the T spd orbitals proceeds largely as before: eight of the nine raMOs correspond to electron pairs centered on the Co atom, with the Co $4p_z$ showing signs of greater delocalization (see Figure S7). Co−Co interactions can also be perceived in these functions, leading us to create sp^2d hybrids corresponding to four Co−Co isolobal bonds. This accounts for 12 of the 16 electrons per formula unit in CaCoSiH, with the contributions from these functions dominating the DOS distribution (Figure 6a).

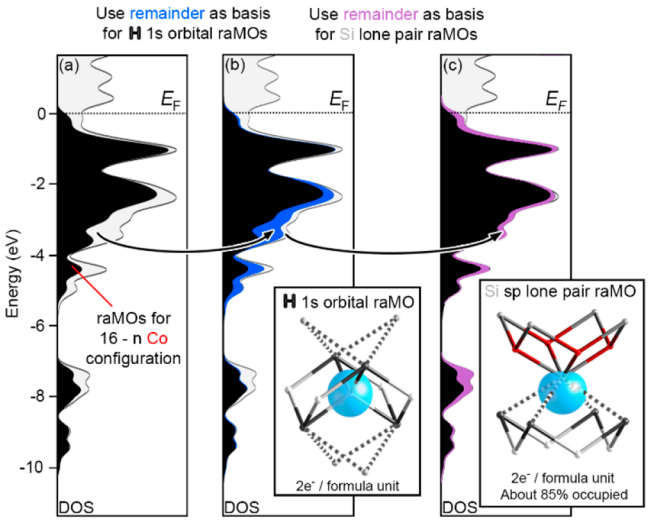

Figure 6. Electron counting in CaCoSiH derived from raMO analysis. First, in (a) the projected DOS distributions for the raMO reconstructions of 16 − *n* (*n* = 4) configurations on the Co atoms. The projected DOS is then augmented by the contributions from raMO recreations of (b) the H 1s orbitals and (c) Si lone pairs on 108 of the 128 Si sites in the supercell used for the analysis. In (b) and (c) raMOs are shown in the insets, with red, light gray, dark gray, and white being used for Co, Si, Ca, and H, respectively.

The remaining electrons are then expected to be distributed over the Si lone pairs and the H 1s orbitals. From the projected DOS curves created for raMOs based on the Si lone pairs and H 1s orbitals, it is clear that the Si lone pair functions contribute more greatly to the states near the E_F, and as such are more likely to exhibit partial occupation. We thus proceed with the full reconstruction of the H 1s orbitals one-by-one, with each resulting raMO function corresponding to the electron pair in an H^- anion. As can be seen in the final reconstructed hydride raMOs (Figure 6b), these functions are tightly localized to the H center, accounting for 2 of the remaining 4 electrons per formula unit.

The obvious place to look for the last two electrons is on the Si lone pair positions. A raMO reconstruction of these functions (following the generation of the all Co- and H-centered electron pairs) proceeds well for 108 of the 128 Si atoms in the supercell of the raMO analysis (Figure 6c), showing features analogous to their counterparts in CaRuSi.

DOI: 10.1021/acs.inorgchem.8b03539
Inorg. Chem. 2019, 58, 2848−2855

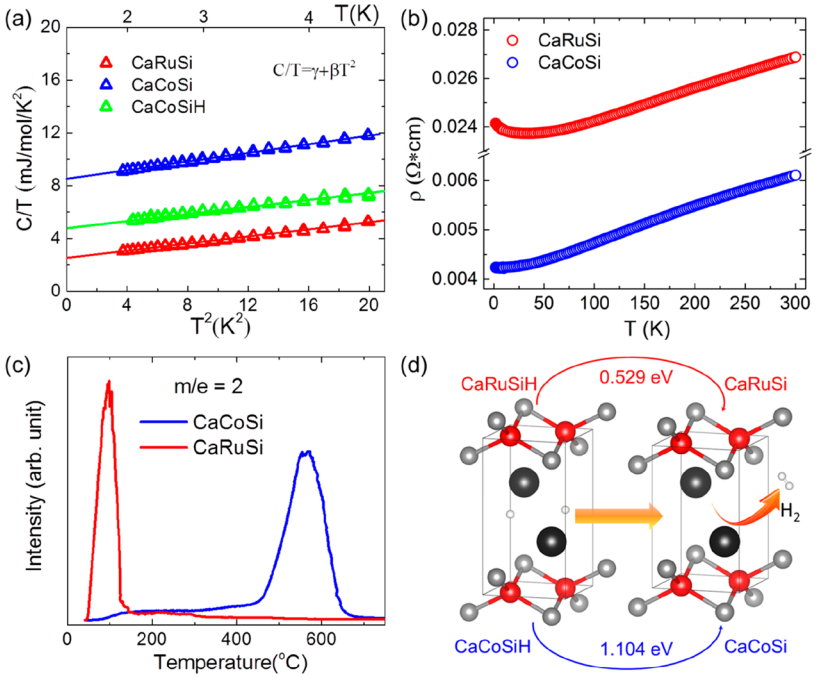

Figure 7. Physical and chemical properties of CaRuSi, CaCoSi, and their hydrides. (a) Low-temperature heat capacity plotted as C/T versus T^2 for CaRuSi, CaCoSi, and CaCoSiH. (b) Electrical resistivity data for CaRuSi and CaCoSi. (c) Hydrogen desorption results measured by thermal desorption spectroscopy (TDS) at a specific mass-to-charge ratio (m/z = 2). (d) The energy change of hydrogen desorption for CaRuSiH and CaCoSiH at 0 K obtained by DFT calculations.

Reconstructions of the remaining Si lone pairs are then more delocalized, and functions with Co-d/Co-d antibonding character begin to emerge. Roughly 1.7 of the final 2 electrons can then be placed in the Si functions, with the remaining electrons being harder to localize.

These features of the electronic structure of CaCoSiH can be understood by considering its formation from the hydrogenation of CaCoSi. CaCoSi is a 15-electron phase, with one electron in excess of the ideal 14-electron count. Upon adding H, the creation of H^- anions provides the opportunity to remove this excess of electrons in the CaCoSi host lattice, making the H atoms effectively hole donors. The persistence of a small amount of Co−Co antibonding contributions to the occupied states of CaCoSiH and the fractional occupancy for the Si-based functions suggest that some of these electrons are instead pulled from the Si lone pairs.

Trends in Physical Properties. To corroborate the electronic structure results obtained theoretically, we measured various physical properties of CaRuSi, CaCoSi, and CaCoSiH. In accord with the Debye model, the low-temperature heat capacities of the phases (Figure 7a) are well-fit with functions of the form $C/T = \gamma + \beta T^2$, where γ is the Sommerfeld parameter and β is the parameter of the Debye T^3 term.[35] As has been shown for other intermetallic phases, the electronic DOS values at the E_F, $N(E_F)$, can then be derived from the intercept γ via $\gamma = 1/3\ \pi^2 N(E_F) k_B^2$ for comparison with those of DFT calculations.[35,36] Here, we obtain $N(E_F)$ values of 1.19, 3.58, and 2.04 eV^{-1} for CaRuSi, CaCoSi, and CaCoSiH, respectively, whose agreement with the theoretical results of Figure 2 provides experimental evidence that electron counts of 14/TSi unit are associated with pseudogaps at the E_F.

Figure 7b shows the resistivity of CaRuSi and CaCoSi measured after pelletizing the samples without further heat treatment. The lower resistivity of CaCoSi is consistent with it having a larger $N(E_F)$ than CaRuSi. It should be noted, however, that, in the pelletized sample, electrons are expected to suffer strong scattering from defects and grain boundaries, and as a result the resistivity values shown are likely much larger than the intrinsic ones. The resistivity data for CaRuSi shows an upturn at low temperatures (below 35 K), suggesting weak localization. Contributions to this metal−insulator−transition (MIT) behavior from a Kondo effect were excluded by magnetization experiments, where no magnetic impurities were observed (Figure S8a). Furthermore, by annealing the pellet at 600 °C for 30 h, the MIT disappeared (Figure S8b), indicating that the factors leading to weak localization, perhaps lattice disorder, were removable through heat treatment. In fact, the annealing reduced the laminated morphology of the sample (Figure S8c), confirming that the process led to grain growth.

Trends in Hydrogen Affinity. Not only the physical properties, but also the chemical properties are largely affected by the 14-electron pseudogap. Although both CaRuSi and CaCoSi absorbed 1H/f.u. to form the corresponding hydrides, the thermal desorption spectroscopy curves for H_2 are dramatically different for the two compounds (Figure 7c). The onset of pronounced H_2 desorption occurs at temperatures almost 300 C° lower for CaRuSi than for CaCoSi, revealing that hydrogen is less stable in the former than in the latter. This can be rationalized from their electronic structures, where CaCoSi has one electron/f.u. in excess of a pseudogap that could be donated to hydrogen to form H^-, while in CaRuSi the formation of H^- requires electrons be drawn from states below the pseudogap. Such a situation is also revealed by the larger and deeper energy states of hydrogen in CaCoSiH relative to the E_F than in its Ru analogue (Figure 2c, Figure 6, and Figure S9). To further confirm the thermal stability of

DOI: 10.1021/acs.inorgchem.8b03539
Inorg. Chem. 2019, 58, 2848−2855

hydrogen in the two compounds, we calculated the energy change for hydrogen desorption at 0 K, e.g., $\Delta E(\mathrm{CaRuSiH}) = 2E(\mathrm{CaRuSi}) + E(\mathrm{H_2}) - 2E(\mathrm{CaRuSiH})$. As indicated in Figure 7d for calculations based on the experimental structures of CaRuSi and CaCoSi,[37] hydrogen desorption requires twice as much energy for CaCoSiH as for CaRuSiH.

Overall, these trends are simply connected to the pseudogap at 14 electrons/TSi unit. CaCoSi goes from having excess electrons to a well-optimized 14-electron count upon forming CaCoSiH, while CaRuSi goes from a 14-electron system to an electron-poor system upon forming CaRuSiH. As a result the CaCoSi exhibits a much greater affinity for hydrogen. This control of H bonding strength from electron count considerations could be useful for the fields of hydrogen storage and hydrogen related catalysis, where different applications require an appropriate binding strength of hydrogen.[13,38−40]

CONCLUSIONS

In summary, we have synthesized a new ternary compound, CaRuSi, and confirmed its tetragonal CeFeSi-type structure with powder X-ray diffraction measurements. A combination of DFT calculations and heat capacity measurements on CaRuSi, CaCoSi, and their hydrides revealed that electron counts of 14 per formula unit are correlated with an electronic pseudogap of the DOS near E_F. The 14-electron pseudogap and its chemical origin were interpreted from the viewpoint of orbital interactions using raMO analysis. The 14 electrons correspond to the filling of one Si lone pair (2 electrons) and T (T = Ru or Co) $16 - n$ configurations (12 electrons), with the support of 4 isolobal T−T bonds around each T atom. We showed that the 14-electron pseudogap has a profound effect on the chemical properties of the phases, with hydrogen desorption experiments demonstrating that CaRuSi (14 electrons) has a much weaker affinity for hydrogen than CaCoSi (15 electrons). While the properties of CaRuSi itself are rather trivial, it opens a simple relationship between electronic structure and properties, both physical and chemical, in ATX compounds that may facilitate the design of materials for superconductivity, hydrogen storage, and catalysis. In particular, it illustrates the opportunities electronic pseudogaps offer for tuning the hydrogen absorption/desorption behavior of intermetallic phases.

ASSOCIATED CONTENT

Supporting Information

The Supporting Information is available free of charge on the ACS Publications website at DOI: 10.1021/acs.inorgchem.8b03539.

Tables for calculation parameters; tables for experimental obtained lattice and structure parameters; additional crystal structures and powder X-ray diffraction patterns for CaRuSiH, CaCoSi, and CaCoSiH; additional calculation results; and additional physical properties (PDF)

AUTHOR INFORMATION

Corresponding Authors

*E-mail: danny@chem.wisc.edu.
*E-mail: hosono@msl.titech.ac.jp.

ORCID

Jiazhen Wu: 0000-0002-6417-8495
Yangfan Lu: 0000-0003-2084-9549
Masaaki Kitano: 0000-0003-4466-7387
Daniel C. Fredrickson: 0000-0002-3717-7008

Author Contributions

⊥J.W. and E.L. contributed equally.

Notes

The authors declare no competing financial interest.

ACKNOWLEDGMENTS

This work was supported by the Japan Society for the Promotion of Science (JSPS) through a Grant-in-Aid for Scientific Research (S), no. 17H06153. E.L. and D.C.F. gratefully acknowledge the financial support of the National Science Foundation through Grant DMR-1809594. Y.L. acknowledges the support of JSPS fellowship for young scientists, no. 18J00745.

REFERENCES

(1) Gupta, S.; Suresh, K. G. Review on Magnetic and Related Properties of RTX Compounds. *J. Alloys Compd.* **2015**, *618*, 562−606.
(2) Pöttgen, R.; Johrendt, D. Equiatomic Intermetallic Europium Compounds: Syntheses, Crystal Chemistry, Chemical Bonding, and Physical Properties. *Chem. Mater.* **2000**, *12*, 875−897.
(3) Hlukhyy, V.; Siggelkow, L.; Fässler, T. F. From One to Three Dimensions: Corrugated $_\infty^1$[NiGe] Ribbons as a Building Block in Alkaline Earth Metal Ae/Ni/Ge Phases with Crystal Structure and Chemical Bonding in AeNiGe (Ae = Mg, Sr, Ba). *Inorg. Chem.* **2013**, *52*, 6905−6915.
(4) Tapp, J. H.; Tang, Z.; Lv, B.; Sasmal, K.; Lorenz, B.; Chu, P. C. W.; Guloy, A. M. LiFeAs: An Intrinsic FeAs-Based Superconductor with T_c = 18 K. *Phys. Rev. B: Condens. Matter Mater. Phys.* **2008**, *78*, 060505.
(5) Paglione, J.; Greene, R. L. High-Temperature Superconductivity in Iron-Based Materials. *Nat. Phys.* **2010**, *6*, 645−658.
(6) Kamihara, Y.; Watanabe, T.; Hirano, M.; Hosono, H. Iron-Based Layered Superconductor La[$O_{1-x}F_x$]FeAs (x = 0.05−0.12) with T_c = 26 K. *J. Am. Chem. Soc.* **2008**, *130*, 3296−3297.
(7) Wang, C.; Wang, Z.; Mei, Y.; Li, Y.; Li, L.; Tang, Z.; Liu, Y.; Zhang, P.; Zhai, H.; Xu, Z.; Cao, G. A New ZrCuSiAs-Type Superconductor: ThFeAsN. *J. Am. Chem. Soc.* **2016**, *138*, 2170−2173.
(8) Chevalier, B.; Gaudin, E.; Tencé, S.; Malaman, B.; Fernandez, J. R.; André, G.; Coqblin, B. Hydrogenation Inducing Antiferromagnetism in the Heavy-Fermion Ternary Silicide CeRuSi. *Phys. Rev. B: Condens. Matter Mater. Phys.* **2008**, *77*, 014414.
(9) Chevalier, B.; Hermes, W.; Heying, B.; Rodewald, U. Ch.; Hammerschmidt, A.; Matar, S. F.; Gaudin, E.; Pöttgen, R. New Hydrides REScSiH and REScGeH (RE = La, Ce): Structure, Magnetism, and Chemical Bonding. *Chem. Mater.* **2010**, *22*, 5013−5021.
(10) Gaudin, E.; Matar, S. F.; Pöttgen, R.; Eul, M.; Chevalier, B. Drastic Change of the Ferromagnetic Properties of the Ternary Germanide GdTiGe through Hydrogen Insertion. *Inorg. Chem.* **2011**, *50*, 11046−11054.
(11) Tencé, S.; Matar, S. F.; André, G.; Gaudin, E.; Chevalier, B. Hydrogenation Inducing Ferromagnetism in the Ternary Antiferromagnet NdCoSi. *Inorg. Chem.* **2010**, *49*, 4836−4842.
(12) Wu, J.; Gong, Y.; Inoshita, T.; Fredrickson, D. C.; Wang, J.; Lu, Y.; Kitano, M.; Hosono, H. Tiered Electron Anions in Multiple Voids of LaScSi and Their Applications to Ammonia Synthesis. *Adv. Mater.* **2017**, *29*, 1700924.
(13) Gong, Y.; Wu, J.; Kitano, M.; Wang, J.; Ye, T.-N.; Li, J.; Kobayashi, Y.; Kishida, K.; Abe, H.; Niwa, Y.; Yang, H.; Tada, T.; Hosono, H. Ternary Intermetallic LaCoSi as a Catalyst for N_2 Activation. *Nat. Catal.* **2018**, *1*, 178−185.
(14) Ye, T.-N.; Lu, Y.; Li, J.; Nakao, T.; Yang, H.; Tada, T.; Kitano, M.; Hosono, H. Copper-Based Intermetallic Electride Catalyst for

DOI: 10.1021/acs.inorgchem.8b03539
Inorg. Chem. 2019, 58, 2848−2855

Chemoselective Hydrogenation Reactions. *J. Am. Chem. Soc.* **2017**, *139*, 17089−17097.
(15) Hoffmann, A. V.; Hlukhyy, V.; Fässler, T. F. Synthesis, Structure, and Chemical Bonding in CaCoSi. *Z. Anorg. Allg. Chem.* **2014**, *640*, 2882−2888.
(16) Rietveld, H. M. A Profile Refinement Method for Nuclear and Magnetic Structures. *J. Appl. Crystallogr.* **1969**, *2*, 65−71.
(17) Larson, A. C.; Von Dreele, R. B. *General Structure Analysis System (GSAS)*; Los Alamos National Laboratory Report, 1994; pp 86−748.
(18) Toby, B. H. EXPGUI, a Graphical User Interface for GSAS. *J. Appl. Crystallogr.* **2001**, *34*, 210−213.
(19) Kresse, G.; Furthmüller, J. Efficient Iterative Schemes for ab Initio Total-energy Calculations Using a Plane-Wave Basis Set. *Phys. Rev. B: Condens. Matter Mater. Phys.* **1996**, *54*, 11169.
(20) Kresse, G.; Furthmüller, J. Efficiency of ab-initio Total Energy Calculations for Metals and Semiconductors Using a Plane-Wave Basis Set. *Comput. Mater. Sci.* **1996**, *6*, 15−50.
(21) Blöchl, P. E. Projector Augmented-Wave Method. *Phys. Rev. B: Condens. Matter Mater. Phys.* **1994**, *50*, 17953.
(22) Kresse, G.; Joubert, D. From Ultrasoft Pseudopotentials to the Projector Augmented-Wave Method. *Phys. Rev. B: Condens. Matter Mater. Phys.* **1999**, *59*, 1758.
(23) Perdew, J. P.; Burke, K.; Ernzerhof, M. Generalized Gradient Approximation Made Simple. *Phys. Rev. Lett.* **1996**, *77*, 3865.
(24) Stacey, T. E.; Fredrickson, D. C. Perceiving molecular themes in the structures and bonding of intermetallic phases: the role of Hückel theory in an ab initio era. *Dalton Trans.* **2012**, *41*, 7801−7813.
(25) Yannello, V. J.; Kilduff, B. J.; Fredrickson, D. C. Isolobal Analogies in Intermetallics: The Reversed Approximation MO Approach and Applications to $CrGa_4$- and Ir_3Ge_7-Type Phases. *Inorg. Chem.* **2014**, *53*, 2730−2741.
(26) Yannello, V. J.; Fredrickson, D. C. Orbital Origins of Helices and Magic Electron Counts in the Nowotny Chimney Ladders: the 18-n Rule and a Path to Incommensurability. *Inorg. Chem.* **2014**, *53*, 10627−10631.
(27) Landrum, G. A.; Glassey, W. V. YAeHMOP: Yet Another extended Hückel Molecular Orbital Package. YAeHMOP is freely available via the Internet at URL: http://yaehmop.sourceforge.net/.
(28) Hlukhyy, V.; Chumalo, N.; Zaremba, V.; Fässler, T. F. Syntheses and Structures of the Germanides CaNiGe and MgCoGe as well as Chemical Bonding in CaNiGe and $CaNi_2Ge_2$. *Z. Anorg. Allg. Chem.* **2008**, *634*, 1249−1255.
(29) Liu, X.; Matsuishi, S.; Fujitsu, S.; Hosono, H. MgFeGe as an Isoelectronic and Isostructural Analog of the Superconductor LiFeAs. *Phys. Rev. B: Condens. Matter Mater. Phys.* **2012**, *85*, 104403.
(30) Liu, X.; Matsuishi, S.; Fujitsu, S.; Ishigaki, T.; Kamiyama, T.; Hosono, H. Layered Hydride CaNiGeH with a ZrCuSiAs-Type Structure: Crystal Structure, Chemical Bonding, and Magnetism Induced by Mn Doping. *J. Am. Chem. Soc.* **2012**, *134*, 11687−11694.
(31) Yannello, V. J.; Fredrickson, D. C. Generality of the 18-n Rule: Intermetallic Structural Chemistry Explained through Isolobal Analogies to Transition Metal Complexes. *Inorg. Chem.* **2015**, *54*, 11385−11398.
(32) Vinokur, A. I.; Fredrickson, D. C. Toward Design Principles for Diffusionless Transformations: The Frustrated Formation of Co−Co Bonds in a Low-Temperature Polymorph of $GdCoSi_2$. *Inorg. Chem.* **2016**, *55*, 6148−6160.
(33) A generalized scheme encompassing the $18 - n$ rule is provided in: (a) Kitahara, K.; Takagiwa, Y.; Kimura, K. Semimetallic Band Structure and Cluster-Based Description of a Cubic Quasicrystalline Approximant in the Al−Cu−Ir System. *J. Phys. Soc. Jpn.* **2015**, *84*, 014703. (b) Kitahara, K.; Takagiwa, Y.; Kimura, K. Unified Cluster-Based Description of Valence Bands in AlIr, $RuAl_2$, $RuGa_3$ and Al-TM Quasicrystalline Approximants. *J. Phys.: Conf. Ser.* **2017**, *809*, 012014.
(34) Albright, T. A.; Burdett, J. K.; Whangbo, M.-H. *Orbital Interactions in Chemistry*, 2nd ed.; Wiley: Hoboken, NJ, 2013; pp 436−464.
(35) Kittel, C. *Introduction to Solid State Physics*, 8th ed.; Wiley: Hoboken, NJ, 2004; pp 141−147.
(36) Aydemir, U.; Candolfi, C.; Ormeci, A.; Oztan, Y.; Baitinger, M.; Oeschler, N.; Steglich, F.; Grin, Yu. Low-Temperature Thermoelectric, Galvanomagnetic, and Thermodynamic Properties of the Type-I Clathrate $Ba_8Au_xSi_{46-x}$. *Phys. Rev. B: Condens. Matter Mater. Phys.* **2011**, *84*, 195137.
(37) Similar hydrogen desorption energies are obtained using the DFT-optimized geometries of the phases, but a weak dependence of the energy on the *c* axis parameter, perhaps due to the layered nature of the compound, leads to *c* for CaCoSi being overly long by ca. 0.40 Å. Curiously, this optimized cell is only ∼5 meV lower in energy than the experimentally determined cell, well within the expected error bar of the DFT calculations.
(38) Züttel, A. Materials for Hydrogen Storage. *Mater. Today* **2003**, *6*, 24−33.
(39) Kitano, M.; Inoue, Y.; Ishikawa, H.; Yamagata, K.; Nakao, T.; Tada, T.; Matsuishi, S.; Yokoyama, T.; Hara, M.; Hosono, H. Essential Role of Hydride Ion in Ruthenium-Based Ammonia Synthesis Catalysts. *Chem. Sci.* **2016**, *7*, 4036−4043.
(40) Kobayashi, Y.; Tang, Y.; Kageyama, T.; Yamashita, H.; Masuda, N.; Hosokawa, S.; Kageyama, H. Titanium-Based Hydrides as Heterogeneous Catalysts for Ammonia Synthesis. *J. Am. Chem. Soc.* **2017**, *139*, 18240−18246.

DOI: 10.1021/acs.inorgchem.8b03539
Inorg. Chem. 2019, 58, 2848−2855